The Astrophysical Journal Supplement Series, 200:12 (15pp), 2012 June doi:10.1088/0067-0049/200/2/12

CfA4: LIGHT CURVES FOR 94 TYPE Ia SUPERNOVAE

Malcolm Hicken[1], Peter Challis[1], Robert P. Kirshner[1], Armin Rest[2], Claire E. Cramer[3], W. Michael Wood-Vasey[4], Gaspar Bakos[1,5], Perry Berlind[1], Warren R. Brown[1], Nelson Caldwell[1], Mike Calkins[1], Thayne Currie[6], Kathy de Kleer[7], Gil Esquerdo[8], Mark Everett[8], Emilio Falco[1], Jose Fernandez[1], Andrew S. Friedman[1], Ted Groner[1], Joel Hartman[1,5], Matthew J. Holman[1], Robert Hutchins[1], Sonia Keys[1], David Kipping[1], Dave Latham[1], George H. Marion[1], Gautham Narayan[1], Michael Pahre[1], Andras Pal[1], Wayne Peters[1], Gopakumar Perumpilly[9], Ben Ripman[1], Brigitta Sipocz[1], Andrew Szentgyorgyi[1], Sumin Tang[1], Manuel A. P. Torres[1], Amali Vaz[10], Scott Wolk[1], and Andreas Zezas[1]

[1] Harvard-Smithsonian Center for Astrophysics, Cambridge, MA 02138, USA; mhicken@cfa.harvard.edu
[2] Space Telescope Science Institute, Baltimore, MD 21218, USA
[3] NIST (National Institute of Standards and Technology), Gaithersburg, MD 20899, USA
[4] Department of Physics and Astronomy, University of Pittsburgh, Pittsburgh, PA 15260, USA
[5] Department of Astrophysical Sciences, Princeton University, Princeton, NJ 08542, USA
[6] NASA, Goddard Space Flight Center, Greenbelt, MD 20771, USA
[7] Department of Physics, Massachusetts Institute of Technology, Cambridge, MA 02139, USA
[8] Planetary Science Institute, 1700 East Fort Lowell Road, Tucson, AZ 85719, USA
[9] Department of Physics, University of South Dakota, Vermillion, SD 57069, USA
[10] Department of Physics, Harvard University, Cambridge, MA 02138, USA
Received 2012 February 14; accepted 2012 April 5; published 2012 May 17

ABSTRACT

We present multi-band optical photometry of 94 spectroscopically confirmed Type Ia supernovae (SNe Ia) in the redshift range 0.0055–0.073, obtained between 2006 and 2011. There are a total of 5522 light-curve points. We show that our natural-system SN photometry has a precision of $\lesssim$0.03 mag in $BVr'i'$, $\lesssim$0.06 mag in u', and $\lesssim$0.07 mag in U for points brighter than 17.5 mag and estimate that it has a systematic uncertainty of 0.014, 0.010, 0.012, 0.014, 0.046, and 0.073 mag in $BVr'i'u'U$, respectively. Comparisons of our standard-system photometry with published SN Ia light curves and comparison stars reveal mean agreement across samples in the range of ∼0.00–0.03 mag. We discuss the recent measurements of our telescope-plus-detector throughput by direct monochromatic illumination by Cramer et al. This technique measures the whole optical path through the telescope, auxiliary optics, filters, and detector under the same conditions used to make SN measurements. Extremely well characterized natural-system passbands (both in wavelength and over time) are crucial for the next generation of SN Ia photometry to reach the 0.01 mag accuracy level. The current sample of low-z SNe Ia is now sufficiently large to remove most of the statistical sampling error from the dark-energy error budget. But pursuing the dark-energy systematic errors by determining highly accurate detector passbands, combining optical and near-infrared (NIR) photometry and spectra, using the nearby sample to illuminate the population properties of SNe Ia, and measuring the local departures from the Hubble flow will benefit from larger, carefully measured nearby samples.

Key word: supernovae: general

Online-only material: machine-readable tables

1. INTRODUCTION

The idea of using supernovae (SNe) as tools for measuring the properties of cosmic expansion has a long history (Kirshner 2010). Pioneering work by the Calan/Tololo survey produced the first large sample of SN Ia light curves, with 29 SN Ia light curves measured with CCD detectors (Hamuy et al. 1996b). Insight from Mark Phillips helped sharpen the use of SNe Ia for distance determinations (Phillips 1993; Hamuy et al. 1996a). At the Harvard-Smithsonian Center for Astrophysics (CfA), we have been engaged in building up the local sample, with 22 SN Ia light curves in the CfA1 sample (Riess et al. 1999), 44 in CfA2 (Jha et al. 2006), and 185 in CfA3 (Hicken et al. 2009a, hereafter H09). Additionally, Krisciunas and colleagues have published a significant number (Krisciunas et al. 2000, 2001, 2003, 2004b, 2004c, 2006), the European Supernova Collaboration has published photometry of various nearby SNe Ia (see Stanishev et al. 2007; Elias-Rosa et al. 2008; Taubenberger et al. 2008, and references therein), and Kowalski et al. (2008) published eight nearby SNe Ia. More recently, the Sloan Digital Sky Survey (SDSS) published 19 SNe Ia with $z < 0.100$ (Holtzman et al. 2008) as part of the SDSS-II program, and the Lick Observatory Supernova Search (LOSS) published optical photometry of 165 SNe Ia (Ganeshalingam et al. 2010). The Carnegie Supernova Project (CSP) produced 35 SN Ia light curves in its first release (Contreras al. 2010, hereafter CSP1) and 50 in its second (Stritzinger et al. 2011, hereafter CSP2), with a majority of these objects including near-infrared (NIR) photometry.

Looking to the future, CfA, LOSS, and CSP continue building further nearby samples. Of particular interest will be ∼100 CfA NIR light curves that have optical photometry from CfA3 and CfA4 (Wood-Vasey et al. 2008; A. Friedman et al. 2012, in preparation). In conjunction with this NIR and optical photometry, the CfA Supernova Group has taken spectra of many of these SNe (Matheson et al. 2008; Blondin et al. 2011; Blondin et al. 2012) using the FAST spectrograph (Fabricant et al. 1998).

From its second and third years, SDSS-II should have photometry of another few dozen spectroscopically confirmed SNe Ia at $z < 0.1$. The Palomar Transient Factory has discovered and spectroscopically confirmed ∼900 SNe Ia in its first two

years,[11] and a large number of these should have quality light curves. The Nearby Supernova Factory (Aldering et al. 2002) has made spectrophotometric observations of several hundred SNe Ia. ESSENCE will shortly publish their whole data set and cosmological analysis (G. Narayan et al. 2012, in preparation). PanSTARRS[12] is also producing large numbers of SN Ia light curves that span the range from low-z to cosmologically telling redshifts with a single photometric system that should diminish the photometric uncertainties encountered by splicing together separate samples at low and high redshift.

In addition to measuring SN data, we have also been engaged in improving the methods for determining SN Ia distances, using observations in multiple photometric bands to estimate both the luminosity of an SN Ia and its extinction (Riess et al. 1996; Jha et al. 2007). MLCS2k2 is the most recent incarnation. SALT2 (Guy et al. 2007) and SiFTO (Conley et al. 2008) are other popular light-curve fitters. The current state of the art uses a statistical model for light-curve shapes that predicts distances to 7% for well-observed SNe Ia using optical data and 5% when NIR photometry is added (Mandel et al. 2011).

The application of the published nearby samples to cosmology includes the determination of H_o to the 3% level from the intercept of the Hubble diagram (Riess et al. 2011), where over half of the SN Ia sample came from CfA3. In addition, the photometry for two of the eight Cepheid-calibrated SNe Ia (SN 2007af and SN 2007sr) came from the CfA3 sample, and the improved photometric calibration of the comparison stars of a third (SN 1995al) was obtained from observations taken at the F. L. Whipple Observatory (FLWO) 1.2 m telescope during the course of the CfA3 observations (Riess et al. 2009). Measurement of q_o has been a major application that requires both high- and low-redshift samples that are on a common photometric system and analyzed in a consistent way. The pioneering work of measuring distant SNe Ia, first published by Riess et al. (1998) and subsequently by Perlmutter et al. (1999), led to the surprising result of cosmic acceleration: $q_o < 0$. Until 2009, the paucity of low-redshift SNe Ia was a significant contributor to the statistical uncertainty in dark-energy properties. This changed in 2009, when Hicken et al. (2009b) used the CfA3 data and data from the literature to construct the Constitution sample of SN Ia redshifts and distances and employed it to improve constraints on the dark-energy equation-of-state parameter, w. The CfA3 sample was also instrumental in providing the data for Kelly et al. (2010), who first detected the small but real relation between SN Ia host-galaxy masses and the residuals from the distance predictions based on SN Ia light curves. This was confirmed at higher redshift by work based on the Sloan SN survey (Lampeitl et al. 2010) and on the Supernova Legacy Survey (Sullivan et al. 2010). A constraint on σ_8, the amplitude of cosmic fluctuations, based in large part on the CfA3 sample, has recently been derived by Turnbull et al. (2012), who used the velocity residuals in the nearby Hubble flow to determine the variance in the dark matter density on a spatial scale of 8 Mpc, $\Omega_m^{0.55}\sigma_{8,\mathrm{lin}} = 0.40 \pm 0.07$.

Amanullah et al. (2010) presented the Union 2.0 set of SN Ia distances, incorporating the CfA3 and first-year SDSS-II photometry (Holtzman et al. 2008), while Suzuki et al. (2012) added 16 cosmologically useful SNe Ia from the Hubble Space Telescope Cluster Supernova Survey, with 10 at $z > 1$, to form the Union 2.1 set and provide tight limits on constant w in a flat CDM model: $1 + w = -0.013^{+0.068}_{-0.073}$, where the uncertainties include all statistical and systematic errors. Sullivan et al. (2011) combine all three years of the Supernova Legacy Survey data with the nearby, first-year SDSS-II and Higher-z (Riess et al. 2007) samples to measure $1 + w = 0.061^{+0.069}_{-0.068}$, where a flat universe is assumed and the uncertainties include all statistical and SN Ia systematic errors. The Union 2.1 and Supernova Legacy Survey measurements of w are the state of the art at the moment.

Since systematic errors in dark-energy properties are now equal to or larger than the errors produced by finite sample sizes, progress demands ways to decrease those systematic errors. Two of the largest sources of systematic uncertainty in using SNe Ia for cosmology are (1) the entanglement of intrinsic SN Ia color and host-galaxy reddening and (2) the overall accuracy of SN Ia photometry, especially in accurately characterizing the passbands used.

One promising path to overcoming the first source of systematic error is through NIR observations of SNe Ia. As shown by Krisciunas et al. (2004a), Wood-Vasey et al. (2008), CSP1, CSP2, and Mandel et al. (2011), SNe Ia are better standard candles in the NIR and extinction by dust is a less vexing problem. The combination of the optical and NIR photometry from the CSP and the CfA will lead to improved disentangling of SN Ia color and host reddening. Another interesting path to better distances and better understanding of the nature of SNe Ia comes through combining information from light curves with information from spectra. Recent work by Blondin et al. (2011) shows that spectra can be used to determine the intrinsic luminosity of SNe Ia from the CfA samples. This builds upon findings by Nugent et al. (1995), Bongard et al. (2006), Hachinger et al. (2008), and Bailey et al. (2009). Silverman et al. (2012) combine nearby SN Ia spectra and photometry to achieve the largest reduction in the Hubble diagram scatter via adding spectra to date. Unlike the broad cosmological problem, the newer areas of combining NIR photometry and optical spectra with optical photometry have significantly less data. This paper, with a sample of 94 new optical light curves, has substantial overlap with CfA NIR photometry (A. Friedman et al. 2012, in preparation) and optical spectra (Blondin et al. 2012) of the same objects. We expect that these measurements will be valuable in developing the tools to improve our knowledge of SNe Ia and of the expansion history of the universe.

The second large source of systematic uncertainty will be greatly reduced through better characterization of detector passbands, as was done for our measurements by C. Cramer et al. (2012, in preparation) using a monochromatic source to determine the system throughput, as described below. In addition to better passband characterization, the significant overlap of nearby SN Ia photometry in the published CfA, LOSS, CSP, and other samples will aid in better understanding any possible systematic photometric effects that a given sample might have.

In Section 2, we describe our observational and data reduction procedures. Greater emphasis is placed on the few differences as compared with the CfA3 procedures, and a briefer description is provided where the procedures remained the same. We then present the CfA4 light curves. In Section 3, we compare the overlapping objects between CfA4, LOSS, and CSP. The CfA4 light curves, comparison star magnitudes, and passbands can be found at our Web site[13] or in the online version of this paper.

[11] http://www.astro.caltech.edu/ptf/

[12] http://pan-starrs.ifa.hawaii.edu/public/science-goals/active-universe.html

[13] http://www.cfa.harvard.edu/supernova/CfA4

2. DATA AND REDUCTION

The CfA4 sample consists of 5522 light-curve points. All 94 SNe have $BVr'i'$ measurements, while 14 have U and 12 have u'. The average number of light-curve points per SN is 14.9 in $Vr'i'$, 12.5 in B, 7.8 in u', and 7.0 in U. The closest redshift, $z_{\rm CMB}$, is 0.0055, and the farthest is 0.073. The median redshift is 0.029, while the 25th and 75th percentile redshifts are 0.017 and 0.038, respectively. Eighty-nine of 94 SNe have $z_{\rm CMB} > 0.010$.

CfA4 data processing followed the same three steps used for CfA3: reduction, calibration, and host-galaxy subtraction. Here we provide a brief overview of the overall process (see H09 for a more detailed treatment) and describe the differences between CfA4 and CfA3 in greater depth. The reduction and subtraction stages were carried out by a version of the ESSENCE and SuperMACHO pipeline (Miknaitis et al. 2007; Rest et al. 2005; Garg et al. 2007). Calibration paralleled CfA3 but was more automated. We employed differential photometry, calibrating the comparison stars surrounding the SN on photometric nights and then measuring the flux of the SN relative to the comparison stars in each data image, on both photometric and non-photometric nights. We employed host-galaxy subtraction for all 94 SNe, using multiple reference images for the majority of the SN.

2.1. Instruments

The CfA4 data were obtained on the 1.2 m telescope at the FLWO using the single-chip, four-amplifier CCD KeplerCam.[14] Observations were acquired on amplifier two with a pixel scale of 0.″672, resulting in a field of view of approximately 11.′5 × 11.′5. The 1.2 m primary mirror deteriorated during the course of the CfA4 observing, and its effects will be described below. A replacement mirror is nearly ready.

Due to the KeplerCam's good cosmetics, a bad-pixel mask was not required. The same $BVr'i'$ filters from CfA3 were used for CfA4. The second of the two CfA3 U filters was used for CfA4 until it broke in 2009 January, and afterward an SDSS u' filter was used. A further description of the filters used in conjunction with the KeplerCam can be found at the FLWO Web site.[15]

2.2. Observations

The CfA Supernova Group depends on both professional and amateur SN searches for its observing targets. Most of these search surveys had typical limiting magnitudes of 19.5 mag. The 1.2 m telescope can reach targets north of declination −20°. The CfA4 discovery data are displayed in Table 1. The reported SN positions are a weighted mean from our subtracted images, usually in r', and are usually an improvement over the announced discovery positions. These positions will be of use for studies requiring more accurate SN positions, such as exploring the host-galaxy properties at the point of explosion. For the reader's convenience we also list the redshift, host-galaxy name, and Milky Way color excess for each SN.

As explained in H09, the CfA Supernova Group rapidly acquires spectra of many of the new SNe brighter than ∼18.5 mag and northward of −20° to provide typing and follow-up investigation. We also begin taking optical and *JHK* photometry. This combination allows for a richer understanding of both individual SNe and the sample as a whole. Priority was usually given to younger and more interesting SNe.

[14] http://linmax.sao.arizona.edu/FLWO/48/kepccd.html
[15] http://linmax.sao.arizona.edu/FLWO/48/CCD.filters.html

The SNe in our sample come from a variety of SN searches. In many cases, the SNe are detected in galaxies that are targeted for monitoring. This means that the host galaxies do not constitute an unbiased sample of the universe, and the properties of the SN in this sample and of their hosts are not necessarily representative. See H09 for further details.

2.3. Pipeline: Reduction Stage

Images underwent bias subtraction and flat fielding. Dome-screen flats were used for $BVr'i'$, while twilight flats were used for Uu'. The i'-band fringes were slightly larger than in CfA3, so fringe corrections were applied. Cosmic rays were removed in the same way as in CfA3.

The UCAC3 catalog (Zacharias 2010) was used to produce a linear astrometric solution for the vast majority of the CfA4 images. The USNO-B1.0 (Monet 2003) or USNO-A2.0 catalogs (Monet 1998) were employed in the few cases where the UCAC3 catalog was too sparse. SWarp (Bertin et al. 2002) was run to properly scale and align the images. DoPHOT (Schechter et al. 1993) was then used to calculate fluxes for all stellar-shaped objects.

2.4. Calibration

We used Landolt (1992) to calibrate our UBV bands and Smith et al. (2002) to calibrate our $r'i'$ bands. For our u' calibration we transformed the Landolt (1992) U magnitudes into u' via the equation $u' = U + 0.854$ (Chonis & Gaskell 2008).

As in CfA3, we performed aperture photometry on the Landolt/Smith standard stars and on our SN-field comparison stars using the NOAO/DIGIPHOT/APPHOT package in IRAF (Tody 1993). Comparison stars were chosen so that they were reasonably well isolated. Due to the deteriorated mirror, which resulted in larger stellar point-spread functions (PSFs), an aperture with radius of 18 pixels was used on both the standard and comparison stars. This was larger than the 15 pixels used in CfA3. An aperture correction was calculated from as many as four bright and isolated stars by subtracting the 6-pixel-radius-aperture magnitude from the 18-pixel-radius-aperture magnitude and applied to the 6-pixel-radius magnitude of all of the stars in the field.

As in CfA3, a linear photometric transformation solution for each night was calculated from our Landolt/Smith stars using the system of Equations (1).

$$\begin{aligned} u - b &= {\rm zp}_{UB} + \alpha_{UB} x + \beta_{UB}(U - B) \\ b - v &= {\rm zp}_{BV} + \alpha_{BV} x + \beta_{BV}(B - V) \\ v - V &= {\rm zp}_{V} + \alpha_{V} x + \beta_{V}(B - V) \\ v - r &= {\rm zp}_{Vr'} + \alpha_{Vr'} x + \beta_{Vr'}(V - r') \\ v - i &= {\rm zp}_{Vi'} + \alpha_{Vi'} x + \beta_{Vi'}(V - i'). \end{aligned} \quad (1)$$

The terms on the left side of the equations are the instrumental colors except for the V-band term. The first term on the right side of each equation is the zero point, followed by the airmass coefficients, α, times the airmass, x. The V-band equation is unique in that it directly relates the instrumental magnitude v to the standard-system magnitude and color, V and $B - V$. The other four equations only relate the instrumental and standard-system colors to each other. The final term on the right of the four color equations multiplies the standard-system color of the standard stars by a coefficient, β, to convert the standard-system color into the natural-system color. When the u' filter replaced the U filter, we used the above equations, replacing U with u'.

Table 1
SN Ia Discovery Data

SN Ia	Position	Galaxy	$z_{\rm helio}$	$z_{\rm CMB}$	$E(B-V)$	$dE(B-V)$	Discovery Reference
2006ct	12:09:56.851 +47:05:44.31	2MASX_J12095669+4705461	0.0315	0.0322	0.0191	0.0014	IAUC 8720
2006ou	11:37:13.039 +15:26:06.59	UGC_6588	0.0135	0.0146	0.0334	0.0016	IAUC 8781
2007A	00:25:16.681 +12:53:12.78	NGC_105	0.0177	0.0165	0.0736	0.0019	CBET 795
2007aj	12:47:54.524 +54:00:38.08	CGCG_270-24	0.0110	0.0115	0.0163	0.0016	IAUC 8822
2007bj	16:22:10.589 −01:30:51.33	NGC_6172	0.0167	0.0170	0.1177	0.0029	IAUC 8834
2007cb	13:58:17.199 −23:22:21.68	ESO_510-G31	0.0366	0.0375	0.0719	0.0011	IAUC 8843
2007cc	14:08:42.050 −21:35:47.50	ESO_578-G26	0.0291	0.0300	0.0794	0.0030	IAUC 8843
2007cf	15:23:07.676 +08:31:45.79	CGCG_77-100	0.0329	0.0335	0.0343	0.0007	IAUC 8843
2007cn	22:13:55.790 +13:45:23.45	UGC_11953	0.0253	0.0241	0.0621	0.0003	IAUC 8851
2007cs	23:49:38.930 +29:55:52.61	UGC_12798	0.0176	0.0164	0.0662	0.0022	CBET 986
2007ev	22:40:06.201 +24:41:56.67	AGC_320702	0.0427	0.0416	0.0490	0.0006	CBET 991
2007fb	23:56:52.383 +05:30:31.90	UGC_12859	0.0180	0.0168	0.0556	0.0011	IAUC 8864
2007fq	20:34:55.742 −23:06:15.38	MCG_-04-48-019	0.0425	0.0416	0.0420	...	CBET 1001
2007fs	22:01:40.450 −21:30:30.22	ESO_601-G5	0.0172	0.0162	0.0336	0.0007	IAUC 8864
2007hg	04:08:32.676 +02:22:43.20	[ISI96]_0405+0214	0.0300	0.0297	0.3799	0.0106	CBET 1047
2007hj	23:01:47.880 +15:35:11.23	NGC_7461	0.0141	0.0129	0.0883	0.0120	IAUC 8874
2007hu	16:56:29.887 +27:58:39.75	NGC_6261	0.0354	0.0354	0.0458	0.0023	CBET 1056
2007if	01:10:51.370 +15:27:39.63	[YQ2007]_J011051.37+152739.9	0.0742	0.0731	0.0831	0.0066	CBET 1059
2007ir	02:33:41.898 +37:40:08.12	UGC_2033	0.0352	0.0345	0.0495	0.0009	CBET 1067
2007is	16:47:14.607 +40:14:36.40	UGC_10553	0.0297	0.0297	0.0201	0.0012	IAUC 8874
2007jg	03:29:50.815 +00:03:24.55	SDSS_J032950.83+000316.0	0.0371	0.0366	0.1065	0.0023	CBET 1076
2007kd	09:25:58.041 +34:38:00.11	MCG_+06-21-36	0.0242	0.0250	0.0217	0.0005	IAUC 8874
2007kf	17:31:31.266 +69:18:39.59	[K2007]J173131.76+691840.1	0.0460	0.0458	0.0439	0.0011	IAUC 8875
2007kg	23:58:37.493 +60:59:07.41	2MFGC_18005	0.0070	0.0063	0.9977	0.0238	IAUC 8875
2007kh	03:15:12.049 +43:10:13.39	[YAA2007a]J031512.10+431013.0	0.0500	0.0495	0.1984	0.0030	CBET 1089
2007kk	03:42:23.258 +39:14:30.30	UGC_2828	0.0410	0.0406	0.2291	0.0132	CBET 1096
2007le	23:38:48.452 −06:31:21.83	NGC_7721	0.0067	0.0055	0.0334	0.0003	CBET 1100
2007nq	00:57:33.721 −01:23:20.29	UGC_595	0.0450	0.0439	0.0354	0.0012	CBET 1106
2007ob	23:12:25.988 +13:54:49.13	2MASX_J23122598+1354503	0.0339	0.0327	0.0681	0.0015	CBET 1112
2007rx	23:40:11.782 +27:25:15.59	BATC_J234012.05+272512.23	0.0301	0.0289	0.0890	0.0078	CBET 1157
2007ss	12:41:06.150 +50:23:28.51	NGC_4617	0.0155	0.0161	0.0149	0.0004	CBET 1175
2007su	22:19:08.884 +13:10:39.89	SDSS_J221908.85+131040.5	0.0279	0.0267	0.0830	0.0006	CBET 1178
2007sw	12:13:36.933 +46:29:36.56	UGC_7228	0.0252	0.0260	0.0186	0.0014	CBET 1185
2007ux	10:09:19.939 +14:59:33.07	2MASX_J10091969+1459268	0.0309	0.0320	0.0448	0.0008	CBET 1187
2008A	01:38:17.394 +35:22:13.06	NGC_634	0.0165	0.0156	0.0542	0.0024	CBET 1193
2008C	06:57:11.469 +20:26:13.58	UGC_3611	0.0166	0.0171	0.0839	0.0026	CBET 1195
2008Q	01:24:57.207 +09:33:01.30	NGC_524	0.0600	0.0590	0.0828	0.0010	CBET 1228
2008Y	11:19:30.581 +54:27:46.21	MCG_+9-19-39	0.0697	0.0703	0.0129	0.0009	CBET 1240
2008Z	09:43:15.258 +36:17:03.64	SDSS_J094315.36+361709.2	0.0210	0.0218	0.0114	0.0007	CBET 1243
2008ac	11:53:45.200 +48:25:20.79	SDSS_J115345.22+482521.0	0.0528	0.0535	0.0190	0.0003	CBET 1245
2008ad	12:49:37.071 +28:19:45.82	ROTSE_J124936.88+281944.8	0.0500	0.0509	0.0130	0.0010	CBET 1245
2008ae	09:56:03.160 +10:29:58.52	IC_577	0.0301	0.0312	0.0277	0.0007	CBET 1247
2008ai	10:57:39.957 +37:39:41.40	CGCG_184-39	0.0353	0.0361	0.0163	0.0010	CBET 1256
2008ar	12:24:37.922 +10:50:16.74	IC_3284	0.0261	0.0272	0.0373	0.0013	CBET 1273
2008at	10:27:12.469 +71:24:55.55	UGC05645	0.0350	0.0352	0.0912	0.0025	CBET 1277
2008bi	08:35:53.388 +00:42:22.85	NGC_2618	0.0134	0.0144	0.0441	0.0014	CBET 1312
2008bw	18:26:50.440 +51:08:16.42	UGC_11241	0.0331	0.0328	0.0399	0.0017	CBET 1346
2008by	12:05:20.907 +40:56:44.43	SDSS_J120520.81+405644.4	0.0450	0.0458	0.0135	0.0002	CBET 1350
2008bz	12:38:57.686 +11:07:45.60	2MASX_J12385810+1107502	0.0603	0.0614	0.0269	0.0021	CBET 1353
2008cd	13:15:01.777 −15:57:06.70	NGC_5038	0.0074	0.0085	0.0688	0.0002	CBET 1360
2008cf	14:07:32.585 −26:33:07.74	[WLF2008]_J140732.38-263305.6	0.0460	0.0469	0.0674	0.0017	CBET 1365
2008cm	13:29:12.826 +11:16:20.65	NGC_2369	0.0111	0.0116	0.1139	0.0013	CBET 1384
2008dr	22:10:51.664 +02:06:29.34	NGC_7222	0.0414	0.0403	0.0428	0.0009	CBET 1419
2008ds	00:29:50.820 +31:23:33.88	UGC_299	0.0210	0.0200	0.0643	0.0028	CBET 1419
2008dt	16:56:30.592 +27:58:33.83	NGC_6261	0.0354	0.0354	0.0458	0.0021	CBET 1423
2008fr	01:11:49.224 +14:38:26.21	SDSS_J011149.19+143826.5	0.0490	0.0479	0.0449	0.0014	CBET 1513
2008gb	02:57:57.141 +46:51:56.19	UGC_2427	0.0370	0.0364	0.1983	0.0041	CBET 1527
2008gl	01:20:54.820 +04:48:19.22	UGC_881	0.0340	0.0330	0.0284	0.0009	CBET 1545
2008hj	00:04:01.913 −11:10:08.35	MCG_-2-1-14	0.0379	0.0367	0.0361	0.0009	CBET 1579
2008hm	03:27:10.889 +46:56:39.20	2MFGC_2845	0.0197	0.0192	0.4425	0.0099	CBET 1586
2008hs	02:25:29.594 +41:50:34.92	NGC_910	0.0173	0.0166	0.0573	0.0004	CBET 1598
2008hv	09:07:34.066 +03:23:32.18	NGC_2765	0.0125	0.0136	0.0321	0.0009	CBET 1601
2009D	03:54:22.817 −19:10:54.56	MCG_-03-10-52	0.0250	0.0247	0.0529	0.0014	CBET 1647
2009Y	14:42:24.563 −17:14:46.70	NGC_5728	0.0093	0.0101	0.1016	0.0006	CBET 1684
2009ad	05:03:33.393 +06:39:35.82	UGC_3236	0.0284	0.0283	0.1120	0.0013	CBET 1694
2009al	10:51:22.049 +08:34:41.98	NGC_3425	0.0221	0.0233	0.0246	0.0005	CBET 1705

Table 1
(Continued)

SN Ia	Position	Galaxy	$z_{\rm helio}$	$z_{\rm CMB}$	$E(B-V)$	$dE(B-V)$	Discovery Reference
2009an	12:22:47.385 +65:51:04.60	NGC_4332	0.0092	0.0095	0.0186	0.0003	CBET 1707
2009bv	13:07:20.517 +35:47:03.20	MCG_+6-29-39	0.0367	0.0375	0.0086	0.0009	CBET 1741
2009dc	15:51:12.083 +25:42:28.43	UGC_10064	0.0214	0.0217	0.0696	0.0017	CBET 1762
2009do	12:34:58.316 +50:51:03.81	NGC_4537	0.0397	0.0403	0.0149	0.0006	CBET 1778
2009ds	11:49:04.025 −09:43:44.48	NGC_3905	0.0192	0.0204	0.0389	0.0007	CBET 1784
2009fv	16:29:44.191 +40:48:41.44	NGC_6173	0.0293	0.0294	0.0063	0.0014	CBET 1834
2009gf	14:15:37.127 +14:16:48.74	NGC_5525	0.0185	0.0193	0.0255	0.0007	CBET 1844
2009hp	02:58:23.938 +06:35:34.64	MCG_+01-08-30	0.0211	0.0204	0.2300	...	CBET 1888
2009ig	02:38:11.613 −01:18:45.52	NGC_1015	0.0088	0.0080	0.0320	0.0009	CBET 1918
2009jr	20:26:26.013 +02:54:31.73	IC_1320	0.0165	0.0156	0.1347	0.0035	CBET 1964
2009kk	03:49:44.320 −03:15:52.66	2MFGC_3182	0.0129	0.0124	0.1376	0.0029	CBET 1991
2009kq	08:36:15.148 +28:04:01.67	MCG_+5-21-1	0.0116	0.0124	0.0410	0.0006	CBET 2005
2009le	02:09:17.160 −23:24:44.74	ESO_478-6	0.0178	0.0170	0.0164	0.0006	CBET 2022
2009lf	02:01:39.616 +15:19:58.13	2MASX_J02014081+1519521	0.0450	0.0441	0.0525	0.0023	CBET 2023
2009li	00:22:51.395 +06:58:11.35	IC_1549	0.0404	0.0392	0.0267	0.0010	CBET 2026
2009na	10:47:01.444 +26:32:37.73	UGC_5884	0.0210	0.0220	0.0319	0.0018	CBET 2098
2009nq	23:15:17.004 +19:01:21.58	NGC_7549	0.0158	0.0146	0.1455	0.0046	CBET 2110
2010A	02:32:39.459 +00:37:09.90	UGC_2019	0.0207	0.0199	0.0291	0.0011	CBET 2109
2010H	08:06:24.342 +01:02:09.01	IC_494	0.0152	0.0160	0.0308	0.0011	CBET 2130
2010Y	10:51:03.994 +65:46:46.40	NGC_3392	0.0109	0.0113	0.0135	0.0015	CBET 2168
2010ag	17:03:53.653 +31:30:06.70	UGC_10679	0.0338	0.0338	0.0309	0.0013	CBET 2195
2010ai	12:59:24.005 +27:59:47.13	SDSS_J125925.04+275948.2	0.0184	0.0193	0.0094	0.0012	CBET 2200
2010cr	13:29:25.082 +11:47:46.49	NGC_5177	0.0216	0.0225	0.0345	0.0014	CBET 2281
2010dt	16:43:15.063 +32:40:27.56	CGCG_168-029	0.0529	0.0529	0.0341	0.0011	CBET 2307
2010dw	15:22:40.279 −05:55:16.46	2MASX_J15224062-0555214	0.0381	0.0387	0.0933	0.0011	CBET 2310
SNF20080522-000	13:36:47.592 +05:08:30.41	SDSS_J133647.59+050833.0	0.0472	0.0482	0.0265	0.0005	SNF site
SNF20080522-011	15:19:58.920 +04:54:16.73	SDSS_J151959.16+045411.2	0.0397	0.0403	0.0427	0.0008	SNF site
PTF10bjs	13:01:11.215 +53:48:57.49	MCG_+9-21-83	0.0300	0.0306	0.0176	0.003	ATEL 2453

Notes. J2000 positions are calibrated against UCAC3 in all but a few cases where there was insufficient coverage and USNO-A2.0 or USNO-B1.0 was used instead. The positions are a weighted mean of our measured SN R.A. and decl., usually from r' but occasionally from V when insufficient r' data were available. These are usually an improvement over the positions reported by the discoverer. The Galaxy column lists the cross-identification object from NED with an underscore replacing any spaces in the name to facilitate the table's use in a columnated format. The redshifts, $z_{\rm helio}$ and $z_{\rm CMB}$, are primarily from NED with a few coming from IAUC/CBET/ATEL sources when none were available from NED. Milky Way $E(B-V)$ values are taken from the NASA IPAC Web site, http://irsa.ipac.caltech.edu/applications/DUST/, except for SN 2007fq and SN 2009hp, which are from the Schlegel et al. (1998) values provided by NED. Finally, the SN discovery reference is listed. The majority are from CBET, IAUC, or ATEL, while two SNe come from the SNF Web site, http://snfactory.lbl.gov/snf/open_access/snlist.php.

The photometric solution was applied to the comparison star measurements. This produced tertiary standards that were used to calibrate the SN measurements in the natural system. To calculate the photometric zero point for each SN image, we took a weighted mean of the differences between our calibrated magnitudes and the instrumental DoPHOT measurements of the comparison stars.

Most of our SN fields were observed on multiple photometric nights to ensure more accurate calibration. However, this was not always possible. All SN fields that were calibrated on only one night had other SN fields calibrated on the same night that were consistent across multiple nights. This increases confidence but does not guarantee the single-night calibrations. The comparison star uncertainties include the measurement uncertainties, the standard deviation of measurements from multiple nights (for single nights, an appropriate error floor was used instead), and the uncertainty of the transformation to the standard system. The typical uncertainty of our V-band comparison star measurements is 0.015 mag.

The color coefficients from each photometric night are plotted in Figure 1. The V, $V-i'$, $U-B$, and $u'-B$ coefficients do not show any significant trend over time and can be fit well by one average value, while the $B-V$ and $V-r'$ coefficients show a step-function distribution with one value in the period before mid-2009 (period one) and another value in the period after (period two). We chose to use 2009 August 15 (MJD = 55058) as the dividing point and calculated average $B-V$ and $V-r'$ color coefficients for period one and another average for period two. The color coefficients are listed in Table 2. The largest difference between the two periods was in the $B-V$ color coefficients, which decreased from 0.93 to 0.87. Since the V-band color

Table 2
Photometric Color Terms

Filter/Time Period	Color Term	Value	Nights
$U-B$/both periods	$(u-b)/(U-B)$	0.9981 ± 0.0209	17
$u'-B$/both periods	$(u-b)/(u'-B)$	0.9089 ± 0.0057	28
$B-V$/period one	$(b-v)/(B-V)$	0.9294 ± 0.0026	38
$B-V$/period two	$(b-v)/(B-V)$	0.8734 ± 0.0024	25
V/both periods	$(v-V)/(B-V)$	0.0233 ± 0.0018	63
$V-r'$/period one	$(v-r)/(V-r')$	1.0684 ± 0.0028	38
$V-r'$/period two	$(v-r)/(V-r')$	1.0265 ± 0.0033	25
$V-i'$/both periods	$(v-i)/(V-i')$	1.0239 ± 0.0016	63

Notes. Lowercase $ubvri$ refer to the instrumental magnitudes, while $Uu'BVr'i'$ refer to the standard magnitudes. All color terms implicitly contain an additive constant. For example, $(v-V) = 0.0233(B-V)$ + const, $(v-i) = 1.0239(V-i')$ + const.

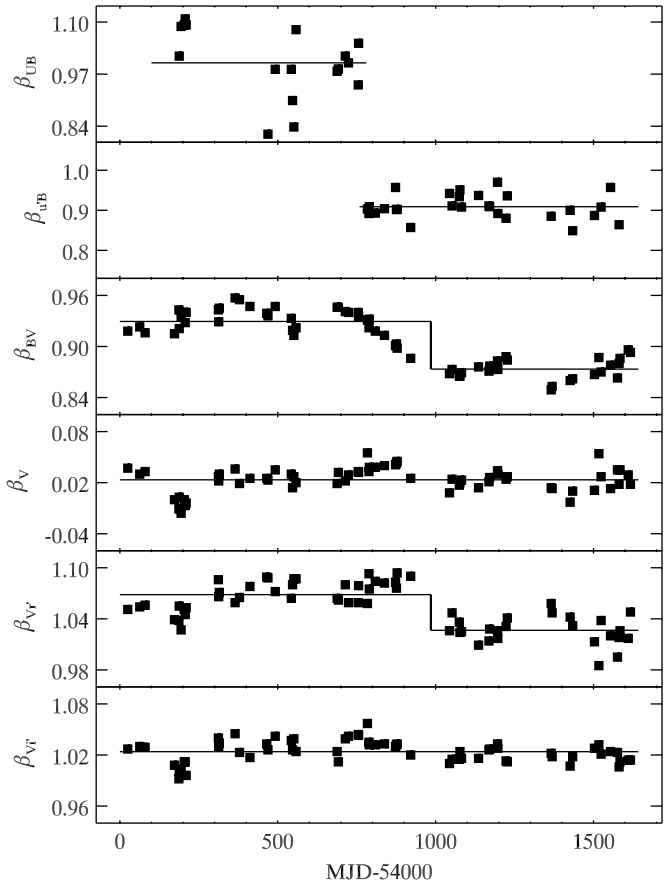

Figure 1. $Uu'BVr'i'$ color coefficients are plotted vs. time with the average value over the relevant time periods shown as a solid line. The $v-V$ and $V-i'$ coefficients are sufficiently stable to be represented by one constant value across the whole time domain, while the $B-V$ and $V-r'$ coefficients are each better described by one value in period one and another value in period two. The $U-B$ coefficients have large uncertainties (not shown) and a large scatter, while the $u'-B$ coefficients have a much smaller scatter, illustrating the superior precision of u' measurements.

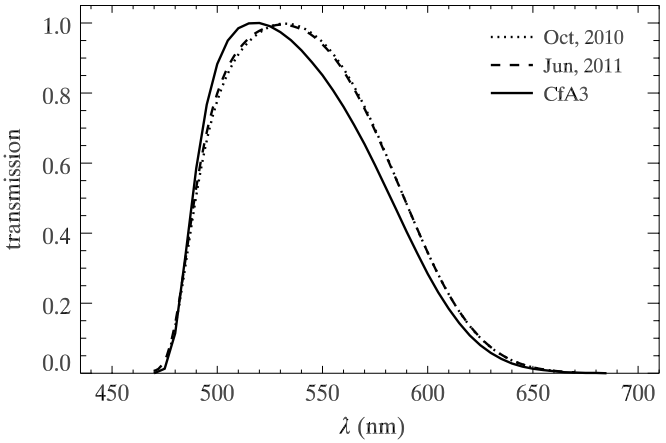

Figure 2. C12 V passbands measured before (dotted) and after (dashed) the 2011 May bakeout are highly consistent with each other and in reasonable agreement with the CfA3 synthetic V passband (solid).

coefficient was stable across the two time periods, this implies that the B passband shifted redward in period two. Deposits or condensation on the camera are likely causes for the changing color coefficients. The KeplerCam was baked on 2011 May 17 to remove deposits/condensation, and the $B-V$ and $V-r'$ color coefficients derived after this returned to their period-one values. However, these post-baking photometric nights were not used for any CfA4 photometric calibration, so only the two time periods, one before and one after 2009 August, with their respective color coefficients were needed. In addition to this, the 1.2 m mirror was deteriorating from 2007 to 2011, losing about 0.6 mag of sensitivity in V. We note that the KeplerCam underwent regular bakeouts every August, but none of these produced a dramatic difference like the one in 2011 May. There is no evidence that the 2011 bakeout procedure was different from previous cycles of desiccation and cleaning, but the result was a significant change in the color coefficients. Whatever the cause, the $B-V$ and $V-r'$ color coefficients returned to their period-one values, and the most likely explanation is that the 2011 May bakeout removed deposits/condensation that previous ones could not.

Synthesized natural-system $BVr'i'$ passbands for the KeplerCam were calculated in H09 by combining the primary and secondary mirror reflectivities (taken as the square of the measured reflectivity of the primary), the measured filter transmissions, and the measured KeplerCam quantum efficiencies. No atmospheric component was included. These passbands were presented as normalized photon sensitivities. No U-band passband was made due to a lack of a U filter transmission curve.

More recently, C. Cramer et al. (2012, in preparation, hereafter C12) measured the FLWO 1.2 m KeplerCam $BVr'i'$ passbands using the technique initially described in Woodward et al. (2010) and Stubbs & Tonry (2006). The dome screen was illuminated with light from a monochromatic, tunable source to generate a series of monochromatic dome flats spanning each filter passband. A NIST-calibrated photodiode[16] monitored the total amount of light incident on the telescope during each exposure. Filter passbands were generated by scaling the camera response to the photodiode signal. The measured passbands therefore include not only the filters, camera, and mirrors, but also the effect of other optics in the telescope optical train—notably, a doublet corrector lens with an aging anti-reflective coating on each of the four surfaces—as well as accumulated dirt and condensation in the camera. The $Vr'i'$ passbands were measured four times: in 2010 July and October and 2011 April and June. The B passband was measured in 2010 October and 2011 April and June. We therefore have measured passbands both before and after the 2011 May bakeout. For more details and tables of the measured passbands, see C12.

The C12 $Vr'i'$ passbands are relatively stable across the bakeout and agree reasonably well with the synthesized CfA3 $Vr'i'$ passbands (see Figure 2 for V), but the C12 pre-bakeout B passband is significantly redward of both its post-bakeout counterpart and the synthesized CfA3 B passband, as seen in Figure 3. The pre-bakeout C12 passbands were observed at two separate times, six months apart, and were virtually identical. The period-two color coefficients were also stable over this same range of time (and longer). The implication is that the pre-bakeout C12 passbands are valid over the period-two time range where the deposits/condensation were present.

After the bakeout, the C12 B passband shifted blueward while the C12 V passband remained stable. This is consistent with the increase of the $B-V$ color coefficients back to the period-one 0.93 level. The post-bakeout C12 B passband can also be seen to be much more consistent with the synthesized CfA3 B passband. We also point out that the CfA3 $B-V$ color coefficient was

[16] http://www.nist.gov/calibrations/upload/sp250-41a.pdf

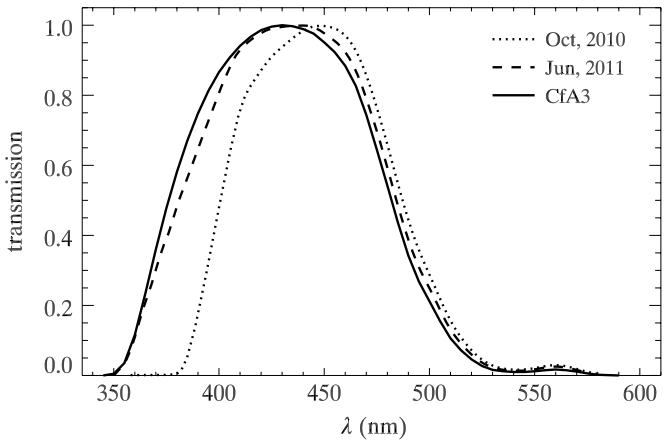

Figure 3. C12 *B* passbands measured before (dotted) and after (dashed) the 2011 May bakeout, showing the blueward shift caused by the bakeout. The CfA3 synthetic *B* passband (solid) agrees fairly well with the post-bakeout C12 *B* passband.

0.92, fairly close to the CfA4 period-one value. These pieces of information suggest that the post-bakeout C12 *B* passband can be used as the CfA4 period-one natural-system *B* passband.

To summarize, the C12 post-bakeout passbands should be used in conjunction with the CfA4 period-one natural-system light curves, while the C12 pre-bakeout passbands should be used for period two. Also, due to the reasonable consistency of the $BVr'i'$ CfA3 and CfA4 period-one color coefficients, the C12 post-bakeout passbands can be used with the CfA3 natural-system light curves. The similarity of the synthesized CfA3 passbands to the C12 $Vr'i'$ and post-bakeout *B* passbands suggests that they were sufficiently accurate and that their use in cosmological studies was satisfactory (Amanullah et al. 2010; Suzuki et al. 2012; Sullivan et al. 2011).

2.5. Pipeline: Host-galaxy Subtraction

Each of the 94 SNe in the CfA4 sample underwent host-galaxy subtraction. Reference images were acquired on clear nights with good seeing and little or no moon so as to maximize their signal-to-noise ratio. However, due to the poor mirror quality, the images had larger PSF sizes than in CfA3. To combat this, multiple reference images were subtracted from the majority of the data images.

The same subtraction algorithm and software as in CfA3 were used for CfA4. A convolution kernel that transforms the PSF of one image to the PSF of the other was calculated using the algorithm of Alard & Lupton (1998) and Alard (2000), with slight improvements as in Becker et al. (2004) and Miknaitis et al. (2007), and then the subtraction was performed. The SN flux in the difference image was then measured with the DoPHOT PSF from the stars of the unconvolved image.

The natural-system flux normalization for the difference image was chosen from the SN data image as opposed to the reference image. This ensured that the normalization of the SN data would be consistent with the passbands and color coefficients from the same time period.

Noise maps were propagated for both data and reference images and used to calculate a noise map for the difference image. Information from the noise image was combined with the DoPHOT uncertainty and calibration uncertainty to produce the uncertainty of the natural-system SN measurement.

The subtraction process was not always perfect, and this introduced extra uncertainty. Steps were taken to estimate this uncertainty. In the cases where multiple reference images existed and were successfully subtracted from one data image, we had a distribution of values that provided a better estimate of the true SN flux and its uncertainty. The differences in these values were due to differences in the various reference images. In order to arrive at one final light-curve point, the multiple photometry values from each data image were plotted and any extreme outliers were removed. Suppose that N values remain. They are different from each other due to Poisson noise in the host galaxy and sky flux in the reference images and due to slight limitations in convolving every reference image equally well to the data image. We took the median of these N values to be the final light-curve data point. There are also N photometry-pipeline uncertainties associated with each of the N photometry values. To calculate the final light-curve uncertainty for the data point in question, $\sigma_{\rm total}$, the median of the N photometry-pipeline uncertainties (we will call this median $\sigma_{\rm pipe}$) was added in quadrature to the standard deviation of the N photometry values ($\sigma_{\rm phot}$).

Formally, there is a slight double counting of the Poisson noise of the reference images since it is part of the standard deviation of the N photometry values, $\sigma_{\rm phot}$, and is also included in the difference image noise maps. However, this is dwarfed by the size of the other uncertainties and has no significant effect on the size of the final error bars. In $\sigma_{\rm phot}$ the Poisson noise of the reference image is typically much smaller than the uncertainties due to imperfect subtractions. And in the pipeline uncertainty, the combination of the data image noise with the DoPhot and calibration uncertainties is larger than the reference image noise that is taken during dark time with better seeing.

For the cases where only one reference image was successfully subtracted, the light-curve value was simply the single-subtraction value. The uncertainty from the single-subtraction photometry was added in quadrature to an estimate of what the standard deviation would have been had multiple reference images existed. This estimate was based on a quadratic fit of the standard deviations of the multiple-subtraction photometry values versus SN magnitude in a given band at magnitudes fainter than 16 mag. For magnitudes brighter than this a constant but representative value was used. This derived function then gave a reasonable estimate that was easily calculated from the SN magnitude of the single-subtraction point. This function is presented in Table 3.

Having multiple reference images for most of the CfA4 sample is one of the main differences with CfA3. In CfA3, there was only one reference image for most of the SNe and none for some SNe with faraway hosts. The uncertainties for the single reference-image CfA3 photometry were what are here called $\sigma_{\rm pipe}$ for $N = 1$ and are almost certainly an underestimate of the true uncertainty. Future use of the CfA3 sample would benefit by adding an estimate of $\sigma_{\rm phot}$. The function we derived for the CfA4 single reference-image photometry could serve as such an estimate and can be added in quadrature to the quoted CfA3 uncertainties.

It was found that the standard deviation of the N light-curve values was typically on the order of their photometry-pipeline uncertainties. Using multiple reference images increased the accuracy of both the CfA4 light-curve values and their uncertainties. We believe that the final error bars are our best estimate of the true uncertainties.

Our light curves were produced in the natural system and then converted to the standard system by using the color coefficients in Table 2. Figures 4–7 show four of the better-sampled CfA4

Table 3
Estimation of $\sigma_{\rm phot}$ for Single Reference-Image Photometry

Mag	U	u'	B	V	r'	i'
$\leqslant$16.0	0.020	0.020	0.012	0.010	0.010	0.010
16.5	0.030	0.038	0.016	0.013	0.012	0.013
17.0	0.048	0.058	0.024	0.019	0.018	0.019
17.5	0.073	0.081	0.037	0.028	0.026	0.028
18.0	0.105	0.107	0.053	0.041	0.037	0.041
18.5	0.144	0.136	0.074	0.058	0.052	0.056
19.0	0.191	0.168	0.099	0.077	0.070	0.075
19.5	0.245	0.203	0.128	0.100	0.091	0.097
20.0	0.306	0.240	0.162	0.126	0.115	0.122
20.5	0.374	0.281	0.199	0.156	0.142	0.150
21.0	0.450	0.324	0.241	0.189	0.172	0.181

Notes. This estimate of $\sigma_{\rm phot}$ for the $N = 1$ cases was based on a quadratic fit of the standard deviations of the multiple-subtraction photometry values versus SN magnitude in a given band at magnitudes fainter than 16 mag. For magnitudes brighter than this a constant but representative value was used. The CfA3 photometry uncertainties would be improved by adding these values in quadrature.

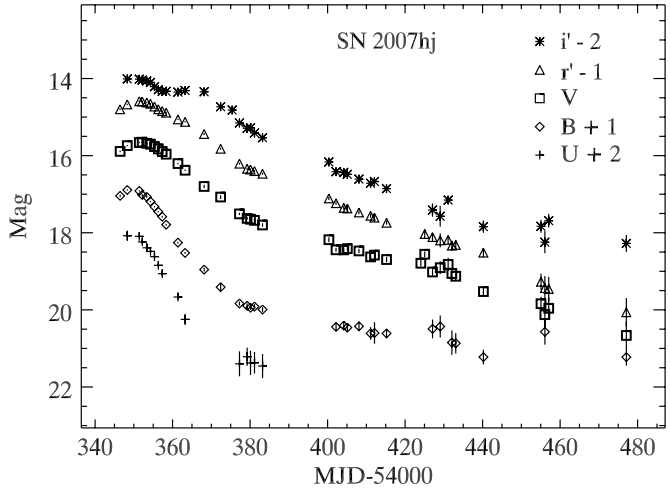

Figure 4. SN 2007hj, one of the better-sampled CfA4 light curves. The error bars are smaller than the symbols for most of the data points.

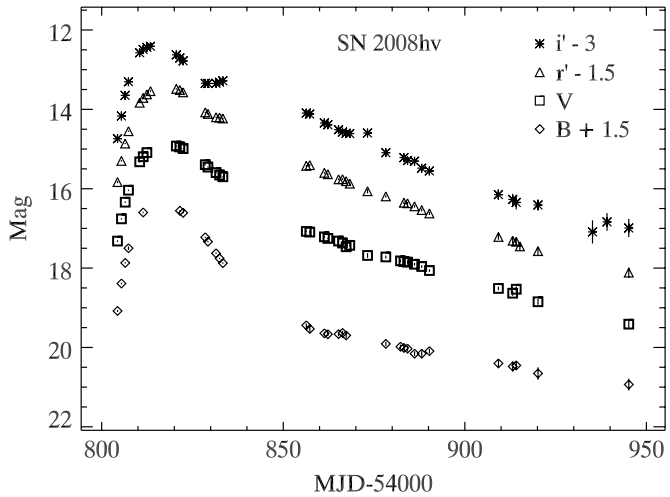

Figure 5. SN 2008hv, one of the better-sampled CfA4 light curves. The error bars are smaller than the symbols for most of the data points.

light curves. The standard-system comparison stars and both natural- and standard-system light curves for all the objects can be found in the online version of Tables 4–6 and at our

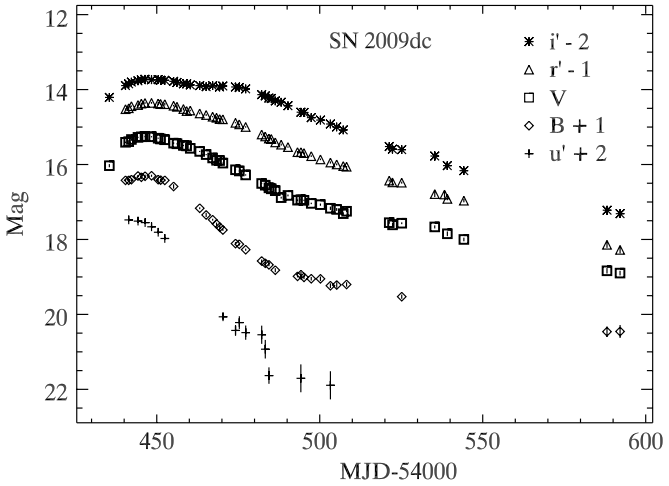

Figure 6. SN 2009dc, one of the better-sampled CfA4 light curves. The error bars are smaller than the symbols for most of the data points.

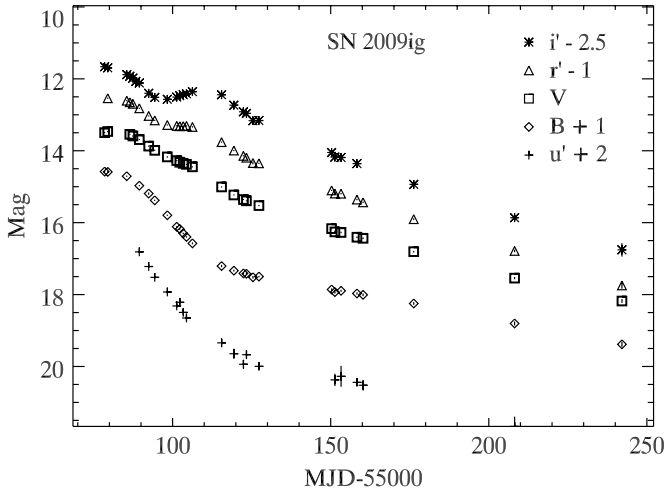

Figure 7. SN 2009ig, one of the better-sampled CfA4 light curves. The error bars are smaller than the symbols for most of the data points.

Web site.[17] The print journal version and astro-ph version of Tables 4–6 only show a small portion of the full data set. The natural-system comparison star photometry is also available at our Web site. For the SN photometry, the number of successful subtractions from a given night that survived outlier rejection is listed. For example, if there were two data images and seven reference images and no photometry points were rejected, then $N = 14$. Usually there was only one data image per night. The uncertainties that were added in quadrature to obtain the final uncertainty are listed. The C12 $BVr'i'$ passbands will be available soon. The natural-system passbands and photometry can be used together to avoid the uncertainty of using star-derived color coefficients for SNe.

We make no effort to estimate the additional uncertainties in the standard-system SN Ia photometry due to the lack of *s*-corrections but note that the uncertainties listed in Table 6 are certainly an underestimate. The natural-system uncertainties are the same as the standard-system uncertainties because we chose not to add the stastistical uncertainty of the color terms, which would increase the total uncertainty to about 1.005 times the natural-system values and are thus negligible. As evident in Table 5, our natural-system SN

[17] http://www.cfa.harvard.edu/supernova/CfA4

Table 4
Standard-system Comparison Star Photometry

SN	Star	R.A.	Decl.	V	σ	N	$U-B$	σ	N	$B-V$	σ	N	$V-r'$	σ	N	$V-i'$	σ	N
2010ai	01	12:59:44.963	+27:56:57.54	15.365	0.015	3	...	...	0	0.837	0.021	3	0.271	0.010	3	0.477	0.015	3
2010ai	02	12:59:41.382	+28:00:07.92	16.715	0.015	7	0.115	0.131	1	0.620	0.019	7	0.185	0.010	7	0.345	0.012	7
2010ai	03	12:59:34.571	+27:54:52.44	17.505	0.013	7	−0.823	0.174	1	0.077	0.020	7	−0.088	0.016	7	−0.281	0.021	7
2010ai	04	12:59:28.781	+27:56:15.51	12.449	0.012	7	...	...	0	1.152	0.016	7	...	...	0	...	...	0
2010ai	05	12:59:26.528	+28:00:24.01	16.656	0.017	7	0.014	0.129	1	0.639	0.019	7	0.157	0.013	7	0.283	0.023	7
2010ai	06	12:59:25.270	+27:59:07.64	17.583	0.015	7	...	...	0	0.527	0.029	7	0.145	0.012	7	0.276	0.030	7
2010ai	07	12:59:24.761	+27:56:24.16	15.921	0.013	7	...	...	0	0.950	0.016	7	0.287	0.009	7	0.474	0.010	7
2010ai	08	12:59:18.650	+28:01:43.34	15.433	0.012	7	...	...	0	1.260	0.016	7	0.497	0.009	7	0.909	0.010	7
2010ai	09	12:59:15.882	+27:57:10.68	16.109	0.013	7	−0.200	0.110	1	0.523	0.018	7	0.113	0.009	7	0.202	0.013	7
2010ai	10	12:59:13.739	+28:02:10.48	16.916	0.013	7	−0.161	0.141	1	0.522	0.018	7	0.124	0.011	7	0.249	0.011	7
2010ai	11	12:59:11.788	+28:00:04.02	15.492	0.012	7	0.302	0.096	1	0.784	0.016	7	0.234	0.009	7	0.398	0.010	7
2010ai	12	12:59:04.168	+28:03:48.67	16.084	0.012	7	0.250	0.110	1	0.761	0.018	7	0.214	0.010	7	0.389	0.012	7
2010ai	13	12:59:01.189	+28:02:03.98	15.265	0.013	7	0.416	0.091	1	0.941	0.017	7	0.293	0.010	7	0.557	0.010	7

Notes. This table presents the CfA4 standard-system comparison star photometry. The complete table is also available from the CfA Web site. The period-one and period-two natural-system values can be calculated by applying the color terms or are available upon request. All $u'-B$ comparison star photometry is presented here and in the complete online version as $U-B$ but can readily be converted to $u'-B$ via the equation $u' = U + 0.854$ (Chonis & Gaskell 2008). The u' SN photometry is presented as u' in Tables 5 and 6.

(This table is available in its entirety in a machine-readable form in the online journal. A portion is shown here for guidance regarding its form and content.)

Table 5
Natural-system SN Photometry

SN	Filter	MJD	N	$\sigma_{\rm pipe}$	$\sigma_{\rm phot}$	Mag	$\sigma_{\rm total}$	Period
2010ai	B	55267.40470	7	0.0240	0.0102	17.2950	0.0261	two
2010ai	B	55268.30587	5	0.0210	0.0227	16.9950	0.0309	two
2010ai	B	55269.37863	7	0.0220	0.0131	16.7740	0.0256	two
2010ai	B	55270.33043	7	0.0200	0.0146	16.5800	0.0248	two
2010ai	B	55275.36791	14	0.0170	0.0185	16.1015	0.0251	two
2010ai	V	55267.40100	7	0.0220	0.0136	17.3110	0.0258	two
2010ai	V	55268.30216	6	0.0215	0.0157	17.0710	0.0266	two
2010ai	V	55269.37493	7	0.0180	0.0108	16.8000	0.0210	two
2010ai	V	55270.32675	7	0.0180	0.0074	16.6190	0.0195	two
2010ai	V	55271.32120	7	0.0160	0.0131	16.4630	0.0207	two
2010ai	r'	55267.39800	6	0.0195	0.0062	17.3215	0.0205	two
2010ai	r'	55268.29912	7	0.0190	0.0098	17.0670	0.0214	two
2010ai	r'	55269.37192	7	0.0190	0.0084	16.7930	0.0208	two
2010ai	r'	55270.32374	7	0.0180	0.0094	16.6060	0.0203	two
2010ai	r'	55271.31818	7	0.0170	0.0077	16.4580	0.0187	two
2010ai	i'	55267.39499	7	0.0260	0.0448	17.5200	0.0518	two
2010ai	i'	55268.29611	7	0.0260	0.0351	17.2520	0.0437	two
2010ai	i'	55269.36892	7	0.0210	0.0240	16.9790	0.0319	two
2010ai	i'	55270.32073	7	0.0220	0.0274	16.8430	0.0351	two
2010ai	i'	55271.31518	7	0.0200	0.0279	16.7490	0.0344	two

Notes. This table presents the CfA4 natural-system SN photometry. The number of successful subtractions from that night that survived outlier rejection is listed in the fourth column. For example, if there were two data images and seven reference images and none were rejected, then $N = 14$. Usually there was only one data image per night. The median of the pipeline-generated uncertainties of the surviving photometry points is listed in the fifth column. The standard deviation of the surviving photometry values for that date is listed in the sixth column. These two values are added in quadrature to produce the total uncertainty. The last column lists what period the photometry belongs to and is of crucial importance so that the corresponding period-one or period-two passbands or color terms are used. Period one is before MJD = 55058 and period two is after. Only the first five nights in each band of one SN are shown here. The complete table with all bands and all SNe is also available from the CfA Web site.

(This table is available in its entirety in a machine-readable form in the online journal. A portion is shown here for guidance regarding its form and content.)

photometry has a precision, $\sigma_{\rm total}$, of $\lesssim$0.03 mag in $BVr'i'$, $\lesssim$0.06 mag in u', and $\lesssim$0.07 mag in U for points brighter than 17.5 mag.

We also estimate a systematic uncertainty in the natural-system photometry of each SN of 0.014, 0.010, 0.012, 0.014, 0.046, and 0.073 mag in $BVr'i'u'U$, respectively. These systematic uncertainties are not included in our natural-system photometry uncertainties in Table 5. They are due to the uncertainties in the zero points of the photometric solution. They were derived by dividing the median uncertainty of all nights' photometric-solution zero points in a given band by the square root of the average number of nights of photometric calibration across all SNe in the same band. For example, the median uncertainty in the V solution is 0.02 mag, and the average number

Table 6
Standard-system SN Photometry

SN	Filter	MJD	N	$\sigma_{\rm pipe}$	$\sigma_{\rm phot}$	Mag	$\sigma_{\rm total}$
2010ai	B	55267.40470	7	0.0240	0.0102	17.2932	0.0261
2010ai	B	55268.30587	5	0.0210	0.0227	16.9861	0.0309
2010ai	B	55269.37863	7	0.0220	0.0131	16.7710	0.0256
2010ai	B	55270.33043	7	0.0200	0.0146	16.5755	0.0248
2010ai	B	55275.36791	14	0.0170	0.0185	16.1004	0.0251
2010ai	V	55267.40100	7	0.0220	0.0136	17.3114	0.0258
2010ai	V	55268.30216	6	0.0215	0.0157	17.0730	0.0266
2010ai	V	55269.37493	7	0.0180	0.0108	16.8007	0.0210
2010ai	V	55270.32675	7	0.0180	0.0074	16.6200	0.0195
2010ai	V	55271.32120	7	0.0160	0.0131	16.4644	0.0207
2010ai	r'	55267.39800	6	0.0195	0.0062	17.3216	0.0205
2010ai	r'	55268.29912	7	0.0190	0.0098	17.0691	0.0214
2010ai	r'	55269.37192	7	0.0190	0.0084	16.7939	0.0208
2010ai	r'	55270.32374	7	0.0180	0.0094	16.6074	0.0203
2010ai	r'	55271.31818	7	0.0170	0.0077	16.4595	0.0187
2010ai	i'	55267.39499	7	0.0260	0.0448	17.5155	0.0518
2010ai	i'	55268.29611	7	0.0260	0.0351	17.2498	0.0437
2010ai	i'	55269.36892	7	0.0210	0.0240	16.9755	0.0319
2010ai	i'	55270.32073	7	0.0220	0.0274	16.8388	0.0351
2010ai	i'	55271.31518	7	0.0200	0.0279	16.7437	0.0344

Notes. This table presents the CfA4 standard-system SN photometry. The number of successful subtractions from that night that survived outlier rejection is listed in the fourth column. For example, if there were two data images and seven reference images and none were rejected, then $N = 14$. Usually there was only one data image per night. The median of the pipeline-generated uncertainties of the surviving photometry points is listed in the fifth column. The standard deviation of the surviving photometry values for that date is listed in the sixth column. These two values are added in quadrature to produce the total uncertainty. Only the first five nights in each band of one SN are shown here. The complete table with all bands and all SNe is also available from the CfA Web site.

(This table is available in its entirety in a machine-readable form in the online journal. A portion is shown here for guidance regarding its form and content.)

of nights is 3.6, resulting in 0.01 mag. These estimates are in rough agreement with the differences between samples seen in Table 7, which also serve as an estimate of the systematic offsets as explained below. The comparison star uncertainties in Table 4 contain this systematic uncertainty, but the photometry pipeline treats them as purely statistical, and so it gets lost due to the relatively large number of comparison stars used for each SN.

3. PHOTOMETRY COMPARISON WITH OTHER SAMPLES

Twelve CfA4 SN Ia light curves overlap with recent LOSS photometry (Ganeshalingam et al. 2010; Silverman et al. 2011), and eight overlap with CSP2. Comparisons between the three groups were made in the standard system. The LOSS and CSP2 comparison star photometry was published in the standard system, as was the LOSS SN photometry. The CSP2 SN photometry was only presented in the natural system. The CSP2 SN standard-system photometry (without *s*-corrections) was provided to us for the overlapping objects (M. Stritzinger 2011, private communication). We emphasize that none of the CfA4, LOSS, or CSP2 standard-system SN photometry is *s*-corrected. Since SN spectral energy distributions (SEDs) differ from the stellar SEDs used to derive the photometric transformation coefficients, the comparisons of the standard-system SN photometry here are limited to providing a reasonable but not highly accurate idea of the agreement between samples. A description of *s*-corrections and why they are needed for more accurate transformation to the standard system is given in Suntzeff (2000). An application of this method is presented in Stritzinger et al. (2002).

Table 7 shows the mean difference of all the comparison stars in common between CfA4, LOSS, and CSP2. There is relatively good agreement (<0.015 mag) in all bands and between all samples except in B, where CSP2 and LOSS differ by 0.035 mag and CSP2 and CfA4 differ by 0.022 mag. The differences in the mean are larger than the standard error of the mean in all cases except for LOSS-CSP2 in V. The comparison star photometry does not require *s*-corrections and gives a good idea of the systematic offsets that would exist between the three groups' SN photometry after accurate *s*-corrections. The mean difference between two groups' photometry can be taken by itself as a good estimate of the systematic offset. Another approach, in the spirit of having $\chi^2 = 1$, is to add enough systematic uncertainty in quadrature to the statistical uncertainty so this total uncertainty is equal to the absolute value of the mean difference. This is only performed when the absolute value of the mean difference is greater than the statistical uncertainty. Following this second approach and assuming that the stars in common are representative of the whole samples suggests that LOSS is systematically brighter than CfA4 by 0.008 mag in B and fainter by 0.011 mag in V. LOSS is 0.034 mag brighter than CSP2 in B and consistent in V. CSP2 would be 0.022 mag fainter than CfA4 in B and 0.015 mag fainter in V. However, it should be noted that there are only ∼80 stars in common between LOSS and CfA4 and between CSP2 and CfA4, and only ∼45 between LOSS and CSP2. Histograms that show all of the comparison star differences are presented in Figures 8–10. The distributions are reasonably symmetric around their mean except for the B LOSS-CSP2 histogram.

In order to compare the SN photometry, a cubic spline was fit to the light curve from one group (for descriptive purposes here, group A). The spline was always of the same order. It was allowed to extend one day beyond the earliest and latest

Table 7
Comparison Star Mean Differences

SN Samples	$\mu_{\Delta B}$	$\sigma/\sqrt{N}$	$\sigma_{\Delta B}$	$N_{\rm stars}$	$\mu_{\Delta V}$	$\sigma/\sqrt{N}$	$\sigma_{\Delta V}$	$N_{\rm stars}$
LOSS−CfA4	−0.0087	0.0037	0.0346	86	0.0109	0.0028	0.0263	86
LOSS−CSP2	−0.0346	0.0071	0.0489	48	−0.0016	0.0048	0.0319	44
CSP2−CfA4	0.0223	0.0032	0.0289	81	0.0149	0.0025	0.0217	77
	$\mu_{\Delta r'}$	$\sigma/\sqrt{N}$	$\sigma_{\Delta r'}$	$N_{\rm stars}$	$\mu_{\Delta i'}$	$\sigma/\sqrt{N}$	$\sigma_{\Delta i'}$	$N_{\rm stars}$
CSP2−CfA4	0.0000	0.0033	0.0300	79	−0.0059	0.0027	0.0236	78

Notes. Listed are the mean, standard error of the mean, and standard deviation of the differences in the photometry of all of the comparison stars in common between CfA4, LOSS, and CSP2. Also provided is the number of comparison stars in common.

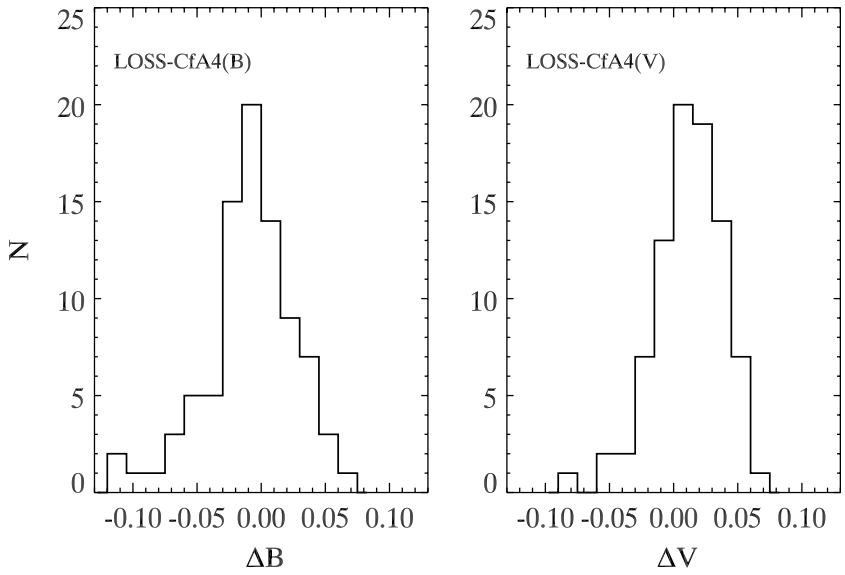

Figure 8. Histograms of the differences in the LOSS-CfA4 BV photometry for all the comparison stars in common between the two samples. The distributions are roughly symmetric.

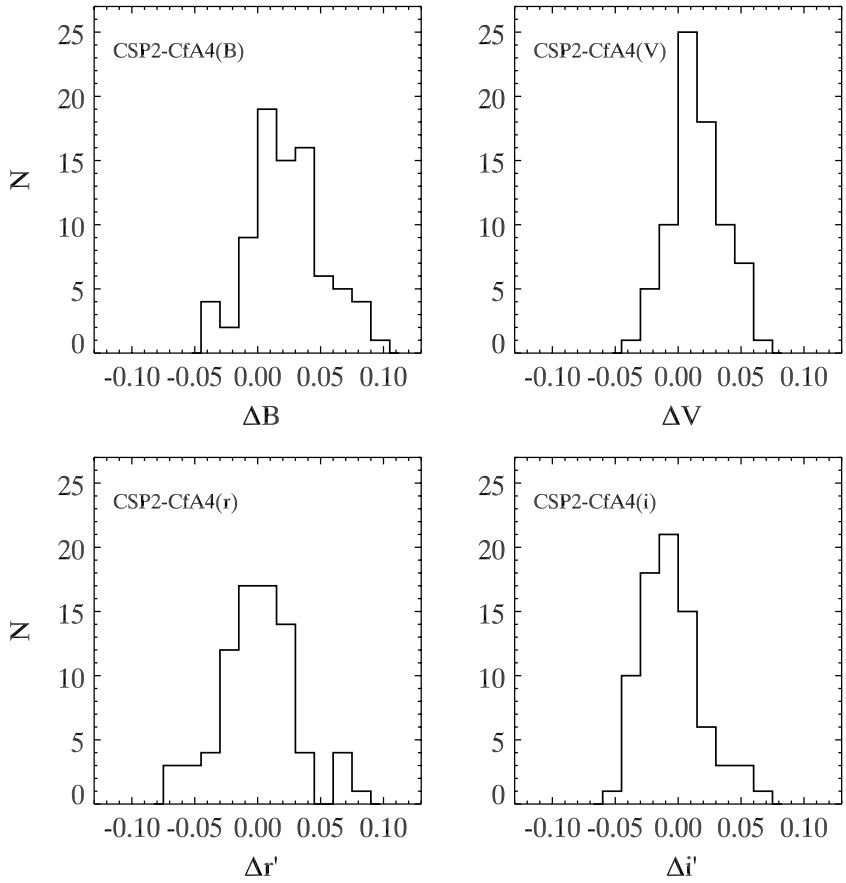

Figure 9. Histograms of the differences in the CSP2-CfA4 $BVr'i'$ photometry for all the comparison stars in common between the two samples. The distributions are roughly symmetric in Vr' with slightly larger tails on the positive side in Bi'.

points. It was visually inspected to ensure that it smoothly fit the data. This spline was then subtracted from the other group's points (group B) that were within the spline's date range and had at least one data point from group A within four days. For each SN that we compared we fit a spline to each group's photometry and subtracted the other group's points. In cases where the light curves of each group are roughly equally well sampled and smooth, there is virtually no difference between which group's data are used for the spline. In these cases we presented the subtraction direction that gave rise to a slightly smaller reduced χ^2. In cases where one group's light curve is more densely sampled and/or smooth, a superior spline fit was produced and we used that one to perform the comparison. In light of the inherent limitations of comparing non-s-corrected

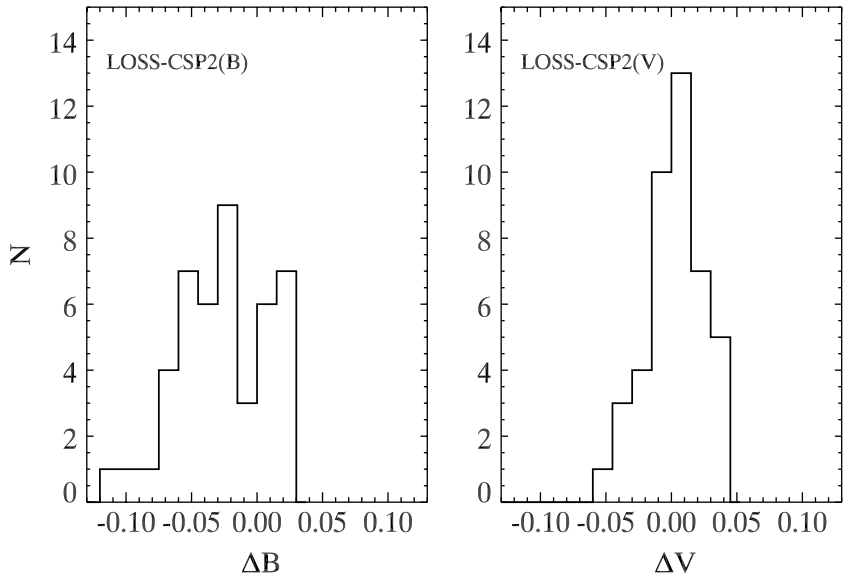

Figure 10. Histograms of the differences in the LOSS-CSP2 BV photometry for all the comparison stars in common between the two samples. The distributions are roughly symmetric in V but not in B.

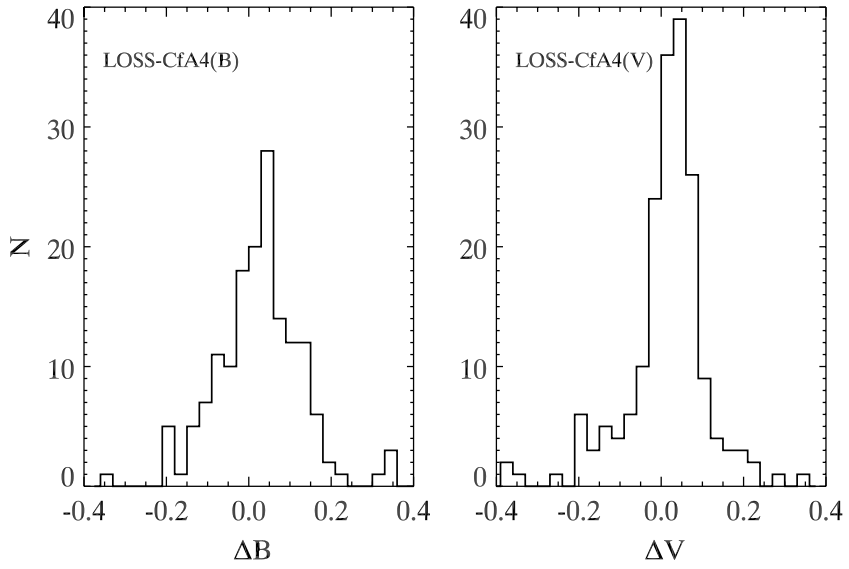

Figure 11. Histograms of the BV differences of the LOSS-CfA4 SN photometry for the 12 SNe in common between the two samples. The distributions are roughly symmetric.

Table 8
Sample-to-Sample SN Photometry Comparisons

SN Samples	$\mu_{\Delta B}$	$\chi^2_\nu(B)$	$\sigma(B)$	$\sigma_{<18}(B)$	$\mu_{\Delta V}$	$\chi^2_\nu(V)$	$\sigma(V)$	$\sigma_{<18}(V)$
LOSS−CfA4	0.036	3.24	0.110	0.075	0.035	3.50	0.099	0.070
CSP2−CfA4	0.027	1.82	0.126	0.035	0.026	3.51	0.095	0.040
	$\mu_{\Delta r'}$	$\chi^2_\nu(r')$	$\sigma(r')$	$\sigma_{<18}(r')$	$\mu_{\Delta i'}$	$\chi^2_\nu(i')$	$\sigma(i')$	$\sigma_{<18}(i')$
CSP2−CfA4	−0.019	3.36	0.096	0.054	0.004	2.37	0.092	0.048

Notes. The weighted mean, reduced χ^2, and standard deviation of all subtractions of the SN photometry in common between CfA4, LOSS, and CSP2. Also, the standard deviation with points fainter than 18 mag is removed.

photometry, which only allows for a reasonable comparison, we opted not to do the slightly more involved task of combining both subtraction directions.

The weighted mean of the differences of all of the subtracted points between two groups in a given band is presented in Table 8. There is general agreement between CfA4, LOSS, and CSP2 in these weighted means. CfA4 is ∼0.03 mag brighter than CSP2 and LOSS in BV, ∼0.02 mag fainter than CSP2 in r', and 0.004 mag brighter than CSP2 in i'. The reduced χ^2 ranges from 1.8 to 3.6. These should be understood as a modified reduced χ^2 since the spline's degrees of freedom were not included in the calculation. The standard deviation of the

Table 9
Comparison Star and SN Photometry Comparison

Samples/SN	μ_Δ	$\sigma/\sqrt{N}$	σ_Δ	$N_{\rm stars}$	$\mu_{\Delta({\rm wgt})}$	χ^2_ν	μ_Δ	$\sigma/\sqrt{N}$	σ_Δ	$N_{\rm stars}$	$\mu_{\Delta({\rm wgt})}$	χ^2_ν
LOSS-CfA4	$B_{\rm stars}$				$B_{\rm SN}$		$V_{\rm stars}$				$V_{\rm SN}$	
2007bj	0.014	0.009	0.028	10	0.0267	2.126	0.019	0.007	0.021	10	0.0500	5.996
2007hj	0.012	0.024	0.058	6	0.0438	3.676	0.019	0.014	0.035	6	0.0438	3.550
2007le	−0.061	0.050	0.071	2	0.0172	3.127	−0.032	0.052	0.074	2	0.0258	2.814
2007ux	0.018	0.007	0.016	5	−0.0788	1.454	0.014	0.008	0.018	5	0.0451	3.148
2008A	−0.021	0.011	0.043	14	0.0568	2.510	0.009	0.007	0.028	14	0.0367	7.460
2008C	−0.022	0.006	0.027	23	−0.0133	0.995	0.017	0.004	0.021	23	0.0295	1.184
2008Q	−0.028	0.006	0.011	3	0.1327	55.403	−0.046	0.005	0.008	3	−0.0013	0.408
2008Z	0.008	0.007	0.016	5	−0.0173	0.659	0.012	0.008	0.019	5	0.0278	5.087
2008ar	−0.002	0.004	0.005	2	0.0537	3.690	−0.010	0.003	0.004	2	0.0126	4.183
2008dr	−0.014	0.006	0.011	3	0.1129	0.647	0.034	0.006	0.011	3	0.0115	0.527
2008dt	−0.001	0.008	0.022	8	−0.0912	0.565	0.008	0.006	0.016	8	−0.1304	4.058
2008ec	−0.016	...	...	1	...	...	−0.009	...	...	1	...	...
2009dc	−0.002	0.007	0.015	4	0.0593	3.314	0.013	0.007	0.014	4	0.0497	3.230
CSP2-CfA4	$B_{\rm stars}$				$B_{\rm SN}$		$V_{\rm stars}$				$V_{\rm SN}$	
2007A	0.016	0.009	0.024	7	0.0156	2.880	0.005	0.005	0.011	5	0.0113	4.647
2007if	0.024	0.011	0.028	7	0.0102	0.819	0.017	0.005	0.014	7	0.0946	3.424
2007jg	0.011	0.004	0.017	15	0.0577	1.167	−0.004	0.005	0.020	14	0.0039	1.462
2007le	0.053	0.008	0.025	9	0.0346	4.573	0.042	0.006	0.017	9	0.0527	10.25
2007nq	0.035	0.002	0.005	5	0.0272	0.876	0.023	0.005	0.011	5	0.0150	1.637
2008C	0.005	0.003	0.013	15	0.0326	2.052	0.028	0.004	0.014	15	0.0227	4.184
2008hv	0.006	0.010	0.033	12	0.0033	1.387	0.005	0.006	0.020	12	−0.0004	1.445
2009dc	0.052	0.007	0.024	11	0.0498	2.364	0.011	0.007	0.021	10	0.0221	1.979
CSP2-CfA4	$r'_{\rm stars}$				$r'_{\rm SN}$		$i'_{\rm stars}$				$i'_{\rm SN}$	
2007A	0.035	0.012	0.032	7	0.0034	1.984	0.023	0.009	0.024	7	0.0108	0.375
2007if	0.005	0.008	0.021	7	0.0345	1.196	−0.001	0.008	0.020	7	0.0301	2.220
2007jg	−0.006	0.004	0.016	14	0.0014	1.352	−0.015	0.005	0.017	13	0.1378	3.892
2007le	0.036	0.008	0.023	9	0.0077	1.005	0.023	0.008	0.024	9	0.0218	2.979
2007nq	0.016	0.005	0.012	5	−0.0286	1.056	−0.004	0.007	0.015	5	0.0281	1.063
2008C	−0.006	0.003	0.012	15	−0.0353	7.983	−0.026	0.002	0.009	15	−0.0369	4.207
2008hv	−0.003	0.005	0.016	12	−0.0460	5.842	−0.008	0.004	0.015	12	−0.0282	3.254
2009dc	−0.047	0.007	0.021	10	−0.0672	7.882	−0.018	0.007	0.022	10	−0.0021	0.527
LOSS-CSP2	$B_{\rm stars}$				$B_{\rm SN}$		$V_{\rm stars}$				$V_{\rm SN}$	
2006bt	0.004	0.010	0.027	7	...	...	0.011	0.008	0.020	7	...	...
2006ej	0.016	...	...	1	...	...	...	...	...	0	...	
2006hb	0.010	0.007	0.015	5	...	...	0.025	0.009	0.018	4	...	...
2007af	−0.038	0.004	0.009	4	...	...	0.012	0.004	0.009	4	...	...
2007bc	−0.107	0.040	0.069	3	...	...	−0.003	0.009	0.013	2	...	...
2007ca	−0.058	0.013	0.028	5	...	...	−0.036	0.006	0.013	5	...	...
2007le	−0.109	0.032	0.064	4	0.0029	2.364	−0.039	0.036	0.072	4	−0.0343	6.137
2008C	−0.018	0.008	0.025	11	−0.0198	3.314	−0.007	0.005	0.018	11	0.0021	1.410
2009dc	−0.044	0.012	0.034	8	0.0030	0.903	0.017	0.006	0.017	7	0.0369	3.767

Notes. Listed are the mean, standard error of the mean, and standard deviation of the differences between comparison stars in common for each SN between CfA4 and LOSS, CfA4 and CSP2, and CSP2 and LOSS, and the number of stars in common. Also listed is the weighted mean and the χ^2 of the differences in the SN photometry.

differences is ∼0.1 mag. This is reduced to 0.04–0.05 mag for the CSP2-CfA4 comparison when points fainter than 18 mag are removed and to 0.07 mag for LOSS-CfA4. A comparison of LOSS versus CSP objects was only performed on the three SNe that were also in common with CfA4. Histograms of the LOSS-CfA4 and CSP2-CfA4 differences for all the subtracted points are shown in each filter in Figures 11 and 12, respectively. The distributions of the differences are all roughly symmetric. The lack of *s*-corrections, to take into account the response of different detectors to SN Ia SEDs, makes the SN photometry comparisons less accurate but still gives a reasonable estimate of how well they agree. Accurate *s*-corrections may resolve some of the discrepancies.

Table 9 presents the comparisons of the individual SNe, showing the mean difference and number of comparison stars in common, as well as the weighted mean and reduced χ^2 of the SN photometry differences. There seems to be very little correlation between the differences in the comparison star and SN photometry between LOSS and CfA4, but there does seem to be between CSP2 and CfA4.

The comparisons of the three SNe Ia in common between CfA4, LOSS, and CSP2 are shown in Table 10. For SN 2007le, the best agreement in V is between LOSS and CfA4 and in B is between LOSS and CSP2. For SN 2008C, the best agreement in V is between LOSS and CSP2 and in B is between LOSS and CfA4. Finally, for SN 2009dc, the best agreement

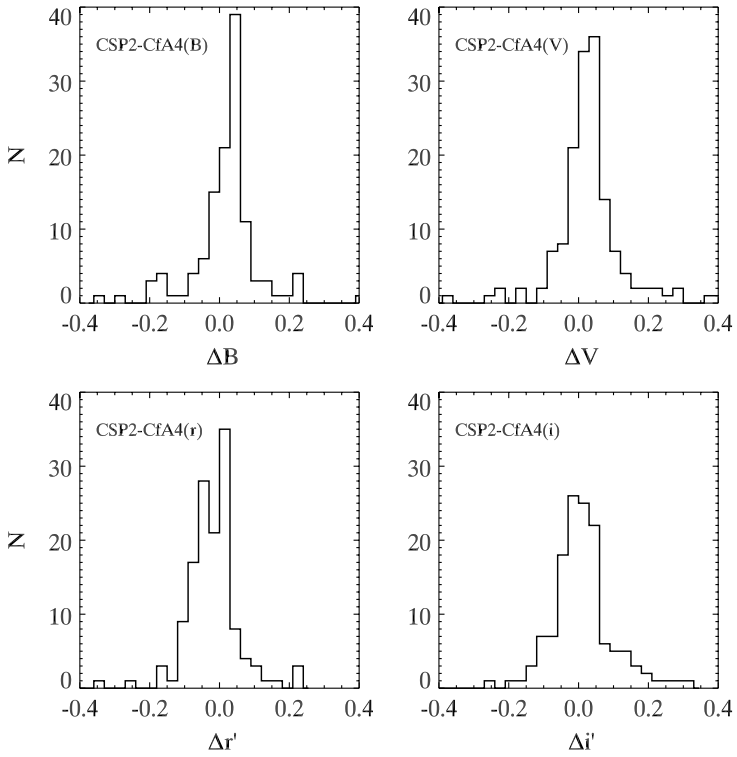

Figure 12. Histograms of the $BVr'i'$ differences of the CSP2-CfA4 SN photometry for the eight SNe in common between the two samples. The distributions are roughly symmetric.

Table 10
Comparing the Three SNe in Common

SN/Samples	μ_Δ	$\sigma/\sqrt{N}$	σ_Δ	$N_{\rm stars}$	$\mu_{\Delta({\rm wgt})}$	σ	χ^2_ν
2007le	$B_{\rm stars}$				$B_{\rm SN}$		
CSP2-CfA4	0.053	0.008	0.025	9	0.0346	0.0340	4.573
LOSS-CfA4	−0.061	0.050	0.071	2	0.0172	0.0521	3.127
LOSS-CSP2	−0.109	0.032	0.064	4	0.0029	0.0434	4.204
2008C	$B_{\rm stars}$				$B_{\rm SN}$		
CSP2-CfA4	0.005	0.003	0.013	15	0.0326	0.1976	2.052
LOSS-CfA4	−0.022	0.006	0.027	23	−0.0133	0.0742	0.995
LOSS-CSP2	−0.018	0.008	0.025	11	−0.0198	0.0226	1.565
2009dc	$B_{\rm stars}$				$B_{\rm SN}$		
CSP2-CfA4	0.052	0.007	0.024	11	0.0498	0.0219	2.364
LOSS-CfA4	−0.002	0.007	0.015	4	0.0593	0.0715	3.314
LOSS-CSP2	−0.044	0.012	0.034	8	0.0030	0.0213	0.903
2007le	$V_{\rm stars}$				$V_{\rm SN}$		
CSP2-CfA4	0.042	0.006	0.017	9	0.0527	0.0201	10.254
LOSS-CfA4	−0.032	0.052	0.074	2	0.0258	0.0385	2.814
LOSS-CSP2	−0.039	0.036	0.072	4	−0.0343	0.0464	6.137
2008C	$V_{\rm stars}$				$V_{\rm SN}$		
CSP2-CfA4	0.028	0.004	0.014	15	0.0227	0.0771	4.184
LOSS-CfA4	0.017	0.004	0.021	23	0.0295	0.0303	1.184
LOSS-CSP2	−0.007	0.005	0.018	11	0.0021	0.0218	1.410
2009dc	$V_{\rm stars}$				$V_{\rm SN}$		
CSP2-CfA4	0.011	0.007	0.021	10	0.0221	0.0168	1.979
LOSS-CfA4	0.013	0.007	0.014	4	0.0497	0.0578	3.230
LOSS-CSP2	0.017	0.006	0.017	7	0.0369	0.0191	3.767

Notes. The mean difference, standard error of the mean, and standard deviation of the comparison star photometry and number of stars in common for each SN Ia are presented in Columns 2 through 5. The weighted mean, standard deviation, and reduced χ^2 of the differences in the SN photometry are presented in the final three columns.

in V is between CSP2 and CfA4 and in B is between LOSS and CSP2.

The main message from these comparisons is that the three groups are in reasonable agreement but that systematic uncertainties and effects are present in both the comparison stars and the SN photometry. A more definitive comparison of the SN photometry would require accurate *s*-corrections.

The primary goal of SN Ia photometry is to produce accurate distances for cosmological purposes. K. Mandel et al. (2012, in preparation) will provide an in-depth analysis of nearby distances that will include all recently published nearby optical and NIR photometry. Part of this will examine offsets between different samples.

4. CONCLUSION

The CfA4 sample consists of 94 nearby SN Ia optical light curves. Most of these are new objects, while 17 of them were also observed by LOSS or CSP2 and have adequate agreement between the different groups. The CfA4 sample is presented in both standard and natural systems. Each of our 94 SN Ia data images had at least one reference image subtracted. In most cases, we had multiple reference images, leading to improved knowledge of the net flux and of its uncertainty. CfA4 is the first large nearby sample to have its natural-system passbands determined by use of a tunable laser and calibrated photodiode (C. Cramer et al. 2012, in preparation). Deposits/condensation on the camera likely caused there to be two time periods with different average $B-V$ and $V-r'$ color coefficients and natural-system passbands. However, the separation of the photometry, calibration, and natural-system passbands into the two time periods takes care of this problem.

Systematic uncertainties are now the largest obstacle in improving understanding of the expansion history of the universe. One of these systematic uncertainties is in the SN Ia photometry

itself. Ensuring stable instruments and understanding the detector passbands involved are critical. In the case of CfA4 the deposits/condensation shifted the passbands, but careful calibrations–both the standard star observations and the C12 passband measurements–enabled this to be understood and overcome.

We thank the staff at FLWO for their dedicated work in maintaining the 1.2 m telescope and instruments. We also thank M. Stritzinger, W. Li, and M. Ganeshalingam for help in comparing the CfA4 sample with the CSP2 and LOSS samples. Finally, we appreciate discussions with K. Mandel. This work has been supported, in part, by NSF grants AST0606772 and AST0907903 to Harvard University.

Facility: FLWO:1.2m

REFERENCES

Alard, C. 2000, A&AS, 144, 363
Alard, C., & Lupton, R. 1998, ApJ, 503, 325
Aldering, G., Adam, G., Antilogus, P., et al. 2002, Proc. SPIE, 4836, 61
Amanullah, R., Lidman, C., Rubin, D., et al. 2010, ApJ, 716, 712
Bailey, S., Aldering, G., Antilogus, P., et al. 2009, A&A, 500, L17
Becker, A. C., Wittman, D. M., Boeshaar, P. C., et al. 2004, ApJ, 611, 418
Bertin, E., Mellier, Y., Radovich, M., et al. 2002, in ASP Conf. Ser. 281, Astronomical Data Analysis Software and Systems XI, ed. D. A. Bohlender, D. Durand, & T. H. Handley (San Francisco, CA: ASP), 228
Blondin, S., Mandel, K. S., & Kirshner, R. P. 2011, A&A, 526, 81
Blondin, S., Matheson, T., Kirshner, R. P., et al. 2012, AJ, 143, 126
Bongard, S., Baron, E., Smadja, G., Branch, D., & Hauschildt, P. H. 2006, ApJ, 647, 513
Chonis, T. S., & Gaskell, C. M. 2008, AJ, 135, 264
Conley, A., Sullivan, M., Hsiao, E. Y., et al. 2008, ApJ, 681, 482
Contreras, C., Hamuy, M., Phillips, M. M., et al. 2010, AJ, 139, 519
Elias-Rosa, N., Benetti, S., Turatto, M., et al. 2008, MNRAS, 384, 107
Fabricant, D., Cheimets, P., Caldwell, N., & Geary, J. 1998, PASP, 110, 79
Ganeshalingam, M., Li, W., Filippenko, A. V., et al. 2010, ApJS, 190, 418
Garg, A., Stubbs, C. W., Challis, P., et al. 2007, AJ, 133, 403
Guy, J., Astier, P., Baumont, S., et al. 2007, A&A, 466, 11
Hachinger, S., Mazzali, P. A., Tanaka, M., Hillebrandt, W., & Benetti, S. 2008, MNRAS, 389, 1087
Hamuy, M., Phillips, M. M., Suntzeff, N. B., et al. 1996a, AJ, 112, 2391
Hamuy, M., Phillips, M. M., Suntzeff, N. B., et al. 1996b, AJ, 112, 2408
Hicken, M., Challis, P., Jha, S., et al. 2009a, ApJ, 700, 331
Hicken, M., Wood-Vasey, W. M., Blondin, S., et al. 2009b, ApJ, 700, 1097
Holtzman, J. A., Marriner, J., Kessler, R., et al. 2008, AJ, 136, 2306
Jha, S., Kirshner, R. P., Challis, P., et al. 2006, AJ, 131, 527
Jha, S., Riess, A. G., & Kirshner, R. P. 2007, ApJ, 659, 122
Kelly, P. L., Hicken, M., Burke, D. L., Mandel, K. S., & Kirshner, R. P. 2010, ApJ, 715, 743
Kirshner, R. P. 2010, in Dark Energy: Observational and Theoretical Approaches, ed. P. Ruiz-Lapuente (Cambridge: Cambridge Univ. Press), 151
Kowalski, M., Rubin, D., Aldering, G., et al. 2008, ApJ, 686, 749
Krisciunas, K., Hastings, N. C., Loomis, K., et al. 2000, ApJ, 539, 658
Krisciunas, K., Phillips, M. M., Stubbs, C., et al. 2001, AJ, 122, 1616
Krisciunas, K., Phillips, M. M., & Suntzeff, N. B. 2004a, ApJ, 602, L81
Krisciunas, K., Phillips, M. M., Suntzeff, N. B., et al. 2004b, AJ, 127, 1664
Krisciunas, K., Prieto, J. L., Garnavich, P. M., et al. 2006, AJ, 131, 1639
Krisciunas, K., Suntzeff, N. B., Candia, P., et al. 2003, AJ, 125, 166
Krisciunas, K., Suntzeff, N. B., Phillips, M. M., et al. 2004c, AJ, 128, 3034
Lampeitl, H., Smith, M., Nichol, R. C., et al. 2010, ApJ, 722, 566
Landolt, A. U. 1992, AJ, 104, 372
Mandel, K., Narayan, G., & Kirshner, R. P. 2011, ApJ, 731, 120
Matheson, T., Kirshner, R. P., Challis, P., et al. 2008, AJ, 135, 1598
Miknaitis, G., Pignata, G., Rest, A., et al. 2007, ApJ, 666, 674
Monet, D. 1998, USNO-A2.0 (11 CD-ROMs; Flagstaff, U.S. Naval Observatory)
Monet, D., Levine, S. E., Canzian, B., et al. 2003, AJ, 125, 984
Nugent, P., Phillips, M., Baron, E., Branch, D., & Hauschildt, P. 1995, ApJ, 455, L147
Perlmutter, S., Aldering, G., Goldhaber, G., et al. 1999, ApJ, 517, 565
Phillips, M. M. 1993, ApJ, 413, L105
Rest, A., Stubbs, C., Becker, A. C., et al. 2005, ApJ, 634, 1103
Riess, A. G., Filippenko, A. V., Challis, P., et al. 1998, AJ, 116, 1009
Riess, A. G., Kirshner, R. P., Schmidt, B. P., et al. 1999, AJ, 11, 707
Riess, A. G., Macri, L., Casertano, S., et al. 2011, ApJ, 730, 119
Riess, A. G., Macri, L., Li, W., et al. 2009, ApJS, 183, 109
Riess, A. G., Press, W. H., & Kirshner, R. P. 1996, ApJ, 473, 88
Riess, A. G., Strolger, L.-G., Casertano, S., et al. 2007, ApJ, 659, 98
Schechter, P. L., Mateo, M., & Saha, A. 1993, PASP, 105, 1342
Schlegel, D. J., Finkbeiner, D. P., & Davis, M. 1998, ApJ, 500, 525
Silverman, J. M., Ganeshalingam, M., Li, W., & Filippenko, A. V. 2012, preprint (arXiv:1202.2130)
Silverman, J. M., Ganeshalingam, M., Li, W., et al. 2011, MNRAS, 410, 585
Smith, J. A., Tucker, D. L., Kent, S., et al. 2002, AJ, 123, 2121
Stanishev, V., Goobar, A., Benetti, S., et al. 2007, A&A, 469, 645
Stritzinger, M., Hamuy, M., Suntzeff, N. B., et al. 2002, AJ, 124, 2100
Stritzinger, M., Phillips, M. M., Boldt, L. N., et al. 2011, AJ, 142, 156
Stubbs, C. W., & Tonry, J. L. 2006, ApJ, 646, 1436
Sullivan, M., Conley, A., Howell, D. A., et al. 2010, MNRAS, 406, 782
Sullivan, M., Guy, J., Conley, A., et al. 2011, ApJ, 737, 102
Suntzeff, N. B. 2000, in AIP Conf. Proc. 522, Cosmic Explosions, ed. S. S. Holt & W. W. Zhang (Melville, NY: AIP), 65
Suzuki, N., Rubin, D., Lidman, C., et al. 2012, ApJ, 746, 85
Taubenberger, S., Hachinger, S., Pignata, G., et al. 2008, MNRAS, 385, 75
Tody, D. 1993, in ASP Conf. Ser. 52, Astronomical Data Analysis Software and Systems II, ed. R. J. Hanisch, R. J. V. Brissenden, & J. Barnes (San Francisco, CA: ASP), 173
Turnbull, S. J., Hudson, M. J., Feldman, H. A., et al. 2012, MNRAS, 420, 447
Wood-Vasey, W. M., Friedman, A. S., Bloom, J. S., et al. 2008, ApJ, 689, 377
Woodward, J. T., Brown, S. W., Lykke, K. R., et al. 2010, Proc. SPIE, 7737, 58
Zacharias, N., Finch, C., Girard, T., et al. 2010, AJ, 139, 2184